43rd ERF, September 12–15, 2017, Milano, IT
580

HELICOPTER-OBSTACLE AERODYNAMIC INTERACTION IN WINDY CONDITIONS

D. Zagaglia*,#, G. Gibertini*, G. Campanardi*, D. Grassi*, A. Zanotti*

*: Politecnico di Milano - Dipartimento di Scienze e Tecnologie Aerospaziali
Campus Bovisa, Via La Masa 34, 20156 Milano, Italy
e–mail: daniele.zagaglia@polimi.it

Keywords: Rotorcraft, Aerodynamics, Vortex Interaction, Particle Image Velocimetry (PIV), Ground Obstacle, Wind Tunnel.

Abstract

The helicopter-obstacle interaction has become a challenging research topic in the last few years. The detrimental effects which can arise in this kind of aerodynamic interaction can be dramatically worsened under windy conditions, particularly when the helicopter flies inside the turbulent and extremely unsteady wake generated by an obstacle. In the present paper a comprehensive experimental survey carried out at Politecnico di Milano is described, obtained by placing a helicopter model in several positions with respect to an obstacle, in windy and not windy conditions. The experimental database comprises load measurements on the rotor in order to assess the rotor performance for different positions with respect to a cubic obstacle, steady and unsteady pressure measurements on the obstacle and Particle Image Velocimetry (PIV) measurements in the region between the rotor and the obstacle in order to highlight the features of the interacting flowfield.

Nomenclature

A	Rotor disc area
c	Blade chord
c_P	Pressure coefficient
c_T	Thrust Coefficient, $T/\left(\rho\Omega^2R^2A\right)$
CIRA	Italian Aerospace Centre
D	Rotor disc diameter
DLR	German Aerospace Centre
GVPM	Galleria del Vento Politecnico di Milano
IGE	In Ground Effect condition
M_{TIP}	Mach Number at blade tip
NLR	Dutch Aerospace Centre
OGE	Out of Ground Effect condition
ONERA	French Aerospace Centre
POLIMI	Politecnico di Milano
PIV	Particle Image Velocimetry
R	Rotor disc radius
Re_{TIP}	Reynolds Number at blade tip, $\Omega Rc/\nu$
V_{IND}	Rotor Induced Velocity
V_∞	Wind velocity
UoG	University of Glasgow
(X, Y, Z)	Absolute reference system
μ	Advance ratio, $V_\infty/(\Omega R)$
Ω	Rotor rotational frequency

1 INTRODUCTION

Helicopters, due to their capability of managing hovering flight, are highly exploited in missions within confined areas. The aerodynamic interaction between the rotor-induced wake and the surrounding obstacles generates, on the one hand, high compensatory workload for the pilot and degradation of aircraft performance, on the other hand unsteady forces which can stress the struc-

ture of the obstacle. These drawbacks can be dramatically worsened under windy conditions, particularly when the helicopter flies inside the turbulent and extremely unsteady wake generated by an obstacle.

Several experimental and numerical investigations have been produced on this topic in the last few years, especially for the Dynamic Interface problem [1], where the helicopter interacts with the superstructures which are usually present on ship decks (see for instance Ref. [2] and [3]). Particle Image Velocimetry (PIV) investigations was adopted by Rajagopalan et al in [4] to acquire 3-component velocity field measurements of the combined wake of a tandem-rotor helicopter and a ship. PIV was also used by Nacakli and Landman in [5] to investigate the recirculation region between a rotor and the vertical wall of a ship deck.

Despite the relative abundance of numerical and experimental work, a systematic study of the aerodynamic phenomena is lacking. The GARTEUR Action Group 22 *"Forces on Obstacles in Rotor Wake"*, comprising several universities (Politecnico di Milano, University of Glasgow, NTUA) and research institutes (CIRA, DLR, ONERA, NLR), originates from the idea of promoting activities which could contribute to a better understanding of these phenomena.

In this framework, the production of an experimental database was carried out initially at Politecnico di Milano (POLIMI) [6], analysing the case of a model helicopter with fuselage interacting with a cuboid obstacle in absence of wind. Following this first experience, the same test rig has recently been tested inside the Large Wind Tunnel of Politecnico di Milano in order to reproduce the case of a helicopter flying in the proximity of a ground structure in windy conditions.

A six-components balance embedded inside the helicopter model allowed to monitor the forces and moments acting on the rotor. The obstacle model presented several pressure taps connected to pressure scanners and high-frequency pressure transducers, in order to allow for both steady and unsteady pressure measurements. Ensemble-averaged PIV was carried out in some relevant configurations in order to observe the interacting flow-field.

2 TEST RIG AND EXPERIMENTAL SETUP

2.1 Test Rig

The test rig that was used during the test campaign at Politecnico di Milano essentially consisted of a helicopter model, inspired by the MD-500, and a parallelepiped obstacle which represented an ideal building, as represented in Figure 1. The helicopter model was held by a horizontal strut fixed to a system of two motorised orthogonal sliding guides to allow the relative position to be changed with respect to the obstacle along the vertical and longitudinal directions of the fuselage. The adopted global reference system (X, Y, Z) is depicted in 1 as well. The X-Z plane is aligned with the mid-span plane of the

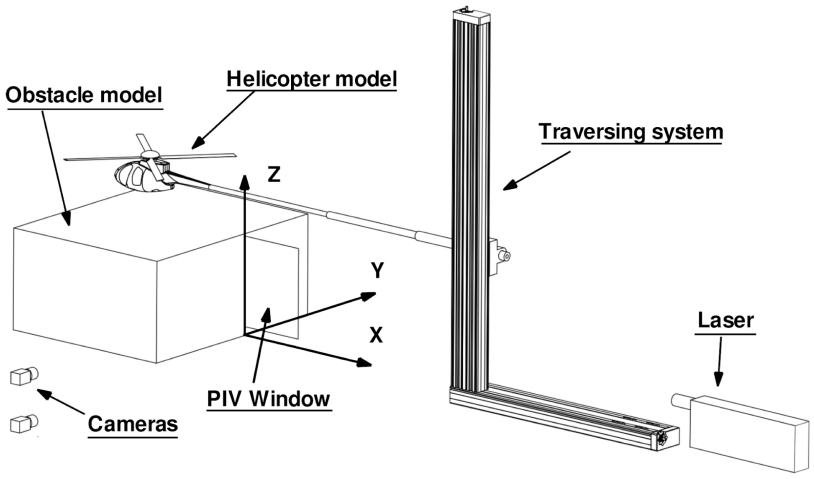

Figure 1: Schematic of the test rig and Reference System

building model and the X-Y plane is aligned with the floor. The origin of the reference system is located on the floor, at the mid-span of the front face.

The rotor had four untwisted and untapered rectangular blades with a chord of $c = 0.032$ m and radius of $R = 0.375$ m. The NACA 0012 airfoil was used. No swash plate was present, so the blade pitch angle was fixed to 10°. A rotational speed of approximately 2580 rpm was maintained during all the tests by means of a brush-less low-voltage electrical motor with an electronic controller. The resulting Mach number and Reynolds number at the blade tip were $M_{\mathrm{TIP}} = 0.30$ and $Re_{\mathrm{TIP}} = 220,000$, respectively. The forces and moments acting on the rotor were measured with a six-component balance nested inside the fuselage. A Hall effect sensor produced one signal per revolution to act as the feedback signal for RPM control.

The building model was a parallelepiped with sharp edges. The dimensions of the parallelepiped were 0.45 m × 0.8 m × 1.0 m. The building model was equipped with 150 pressure taps (see Fig. 2), of which 31 lay on the top plate , 21 lay on the side plate and 48 lay on the front plate. The remaining taps were located on the other three faces, which were not considered in the present study. The pressures were acquired by means of three low-range 32-port scanners by Pressure System Inc. embedded inside the building model and 20 Kulites XCS-093 transducers for the unsteady pressure measurements in selected positions (see Figure 2).

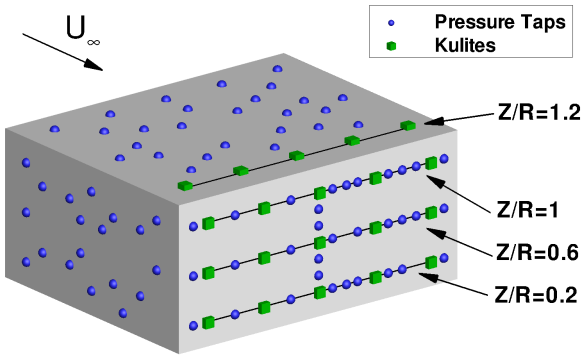

Figure 2: Obstacle model: location of the pressure taps.

Due to the lack of a well-defined dynamic pressure in the wind-off tests, the pressure results will be presented by the pressure coefficient c_P:

$$c_P = \frac{P - P_\infty}{\frac{1}{2}\rho V_{\mathrm{IND}}^2},$$

where P_∞ is the static far-field pressure and V_{IND} is the estimated rotor-induced velocity according to the Momentum Theory (MT) [7] which is defined as:

$$V_{\mathrm{IND}} = V_{\mathrm{TIP}} \sqrt{\frac{c_{T,OGE}}{2}}.$$

The PIV setup is represented in Figure 1. The PIV system comprised a Litron NANO-L-200-15 Nd:Yag double-pulse laser with an output energy of 200 mJ and wavelength of 532 nm, and two Imperx ICL-B1921M CCD cameras with a 12-bit, 1952×1112 pixel array. The laser was positioned on the floor so that the laser sheet was aligned with the X-Z plane . The camera line of sight was positioned perpendicular to the laser sheet. A PIVpart30 particle generator by PIVTEC with Laskin atomizer nozzles was used for the seeding, which consisted of small oil droplets with diameters of 1-2 μm. The image pair analysis was carried out using PIVviev 2C software [8], which was developed by PIVTEC in close cooperation with the PIV-Group of DLR. The results that will be shown are the ensemble-averaged measurements over 400 image pairs.

2.2 Test Matrix

Tests were carried out with the parallelepiped leaned on the 0.8 m × 1 m face to represent a low-rise building. With respect to the fixed reference system (X, Y, Z) shown in Fig. 3, several series of tests consisting of vertical sweeps, where X and Y were constant or horizontal sweeps, where Z and Y were constant, were carried out. For the sake of brevity, only one test (Test T2) will be addressed in the present paper and its features are presented in Table 1. The X, Y and Z coordinates correspond to the position of the rotor hub centre for that particular test.

Test name	Obstacle	Sweep direction	X/R	Y/R	Z/R	First point	Last point	$N°$ of points	μ
T2	YES	X	-	0	2	$X/R = -1$	$X/R = 1$	5	0 / 0.05

Table 1: Test Matrix

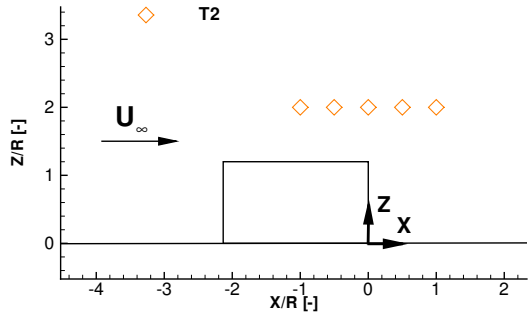

Figure 3: Schematic of the Test Matrix Points

Figure 4: The rotor-obstacle test rig mounted inside the GVPM wind tunnel

The tests were carried out in the large test chamber (suitable for wind engineering tests) of the Large wind tunnel of Politecnico di Milano (GVPM, see ref. [9]), as depicted in Figure 4. The test chamber is 13.84 m wide, 3.84 m high and 38 m long. Despite the huge test chamber, a relatively small model was used in order to prevent any interference effect with the surrounding walls.

The various test were carried out both in the wind-off and wind-on configuration. In particular, a wind velocity corresponding to an advance ratio $\mu = U_\infty/(\Omega R) = 0.05$, in order to simulate the effect of a moderate wind that flows past the obstacle.

3 RESULTS

Test T2 considered a set of points on a horizontal line on the symmetry plane at $Z/R = 2$. As shown in Figure 5, the gradual ground effects that affected the rotor for $\mu = 0$ as the helicopter is moved on the obstacle, is mitigated in windy conditions. The drop in the thrust coefficient with respect to the wind-off case is up to 7% of the OGE value.

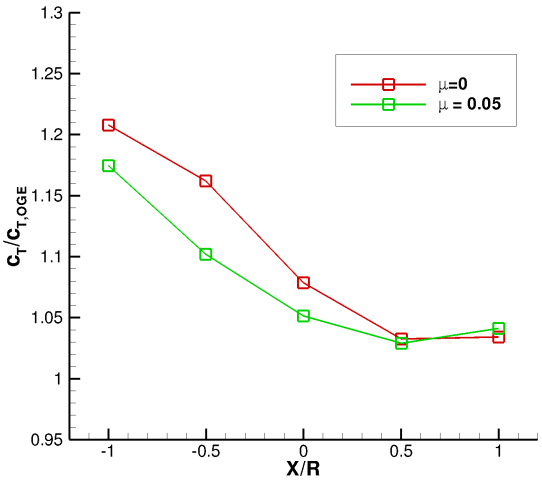

Figure 5: T2-Ratio between the thrust coefficient c_T and the one measured in OGE

Let us now consider the pressure contours of Figure 6. Very significant differences in the pressure patterns can be observed between the wind-off and wind-on condition. When the rotor is placed at $X/R = -1$, Figure 6b, the high-pressure region corresponding to the wake impingement area is moved downstream. Correspondingly a low-pressure region develop before the impingement area. The pressure fluctuations on the upper surface of the obstacle appear to be slightly

mitigated by the wind presence, as it can be appreciated by comparing Figure 7a and 7b.

When the rotor centre lies exactly above the building edge for $X/R = 0$ in the wind off case (Figure 6c), the pressure distributions on the different faces of the building indicate the presence of a complex flow structure that was markedly asymmetrical. The diagonal pattern on the front face is probably related to the helicoidal structure of the rotor wake. When the wind is blowing,(Figure 6d, the pressure pattern on the front face drastically changes with respect to the wind-off case. In particular, the oblique low pressure region is still present, but its peak is less intense and it has moved downwards, approximately at half the height of the obstacle. Consequently the high pressure region on the right of the building looses intensity as well and it is pushed on the left side of the obstacle. The highest time-variability of the pressure coefficient among all test points was measured for this rotor position, both for the wind-off and wind-on case. Let us first consider the test at $\mu = 0$, whose results are shown in Figure 7c. All the taps on the front face experience strong pressure unsteadiness, particularly those in the strong depression area ($Z/R = 1$) and in the high-pressure region, where the standard deviation of the pressure coefficient reaches values up to $\sigma_{c_P} = 1$. The pressure taps on the obstacle upper surface ($Z/R = 1.2$), which are washed by the rotor wake, unexpectedly show very limited σ_{c_P}. However this is not verified anymore for the wind-on condition (Figure 7d), where also the pressure taps on the obstacle upper surface experience large pressure coefficient fluctuations over time.

Eventually when the helicopter model is placed at $X/R = 1$ in the wind-off case,the helicopter effect was only apparent on the front face, where the measured overpressure is caused by the rotor wake that, once deflected by the ground, impinges on lower part of the obstacle, as it can be appreciated in Figure 6e. When the wind is blowing, Figure 6f, the high-pressure region on the lower part of the front face of the building is drastically reduced, both in terms of extension and pressure peak, with respect to the wind-off case, leaving space to a low-pressure region on its upper part. However, the pressure fluctuations grow drastically in the high pressure region on the lower part of the obstacle ($Z/R = 0.2$), as it can be noticed by comparing Figure 7e ($\mu = 0$) and Figure 7f ($\mu = 0.05$).

Test T2 was also investigated by means of Particle Image Velocimetry. Figure 8 presents the velocity field time-averaged over 400 image pairs. The measured flow fields are visualised by means of the in-plane velocity magnitude contours and in-plane streamlines patterns. For the test condition at $X/R = -1$, the flow morphology of the wind-on configuration (Figure 8b) is quite similar to the corresponding wind-off test. However the high-speed layer, originated by the rotor wake deflection, is issued from the upper face of the obstacle with a larger angle with respect to the vertical direction due to the presence of the wind. Greater differences with respect to the wind-off test can be appreciated for $X/R = 0$, Figure 8d, and for $X/R = 1$, Figure 8f. A reduction of the in-plane velocity magnitude in the rotor wake can be appreciated in both cases, probably indicating that the interaction between the rotor and obstacle wakes produces a remarkable dissipation of the rotor wake energy. For the test point at $X/R = 0$, both the aft and fore portion of the rotor wake are more aligned to the wind direction with respect to the wind-off case, as for $X/R = -1$. Eventually for the test condition at $X/R = 1$ (Figure 8f) the fore part of the wake is initially deflected downstream by the wind, but when it reaches the ground it is deflected again in the opposite direction, towards the obstacle, creating an high-pressure region on the lower part of the front face, as already commented for Figure 6f. The reduced pressure peak with respect to the wind off case can indeed be explained by the dissipation in the deflected rotor wake that can be observed in Figure 8f. Moreover, in this case, the interaction creates a clockwise-rotating flow structure near the obstacle, that was non present for $\mu = 0$, where the rotor wake skimmed the obstacle face.

4 CONCLUSIONS

In the present paper, a comprehensive experimental survey on the aerodynamic interaction between a rotor and a model ground obstacle in windy conditions has been described.

The experimental activities were carried out at Politecnico di Milano and University of Glas-

gow and took advantage and experimental techniques. Load measurements on the rotor were carried out in order to assess the rotor performance for different rotor positions with respect to the obstacle. Particle Image Velocimetry (PIV) measurements in the region between the rotor and the obstacle were carried out in order to have a better insight of the interacting flow field. Steady and unsteady pressure measurements on the obstacle allowed a better understanding of the loads that the helicopter creates on the surroundings.

The gradual ground effects that affects the rotor as the helicopter is moved on the obstacle for the wind-off case is mitigated in windy conditions.

From the point of view of the loads on the surroundings, the obstacle experiences remarkable spatial and time-variation of the pressure patterns, strongly dependent on the helicopter position. High pressure regions occur on the obstacle in the regions directly underneath the rotor or in those regions where the rotor wake impinges after being deflected by the ground. These regions are usually also characterised by a fair degree of unsteadiness. When the helicopter model is placed directly over the obstacle edge, the pressure distributions on the front face of the obstacle present a diagonal pattern on the front face, probably due to the helicoidal structure of the rotor wake. This region is characterised by remarkable pressure fluctuations and the presence of contextual high and low-pressure regions. The effect of the wind on the obstacle usually leads to a reduction in the pressure peaks, even though the pressure fluctuations on the obstacle are even magnified in certain positions.

References

[1] SJ Zan. On aerodynamic modelling and simulation of the dynamic interface. *Proceedings of the Institution of Mechanical Engineers, Part G: Journal of Aerospace Engineering*, 219(5):393–410, 2005.

[2] Clement Crozon, Rene Steijl, and George N Barakos. Numerical study of helicopter rotors in a ship airwake. *Journal of Aircraft*, 51(6):1813–1832, 2014.

[3] Christopher H Kri, Yaxing Wang, Gareth D Padfield, James S Forrest, and Ieuan Owen. Aerodynamic loading characteristics of a model-scale helicopter in a ship's airwake. *Journal of Aircraft*, 49(5):1271–1278, 2012.

[4] G. Rajagopalan, S Niazi, A.J. Wadcock, G.K.Yamauchi, and M.J. Silva. Experimental and computational study of the interaction between a tandem-rotor helicopter and a ship. In *American Helicopter Society* 61^{th} *Annual Forum*, June 1-3 2005.

[5] Yavuz Nacakli and Drew Landman. Helicopter downwash/frigate airwake interaction flowfield piv surveys in a low speed wind tunnel. In *AHS 67th annual forum*, pages 1–11, 2011.

[6] Giuseppe Gibertini, Donato Grassi, Cesare Parolini, Daniele Zagaglia, and Alex Zanotti. Experimental investigation on the aerodynamic interaction between a helicopter and ground obstacles. *Proceedings of the Institution of Mechanical Engineers, Part G: Journal of Aerospace Engineering*, 229(8):1395–1406, 2015.

[7] J. Gordon Leishman. *Principles of Helicopter Aerodynamics*, chapter 10. Cambridge University Press, New York, NY, 2000.

[8] PIVTEC. *PIVview 2C version 3.0, User Manual.* available online at www.pivtec.com.

[9] G Gibertini, L Gasparini, and A Zasso. Aerodynamic design of a civil-aeronautical low speed large wind tunnel. In *AGARD conference proceedings*, pages 6–1. AGARD, 1997.

Copyright Statement

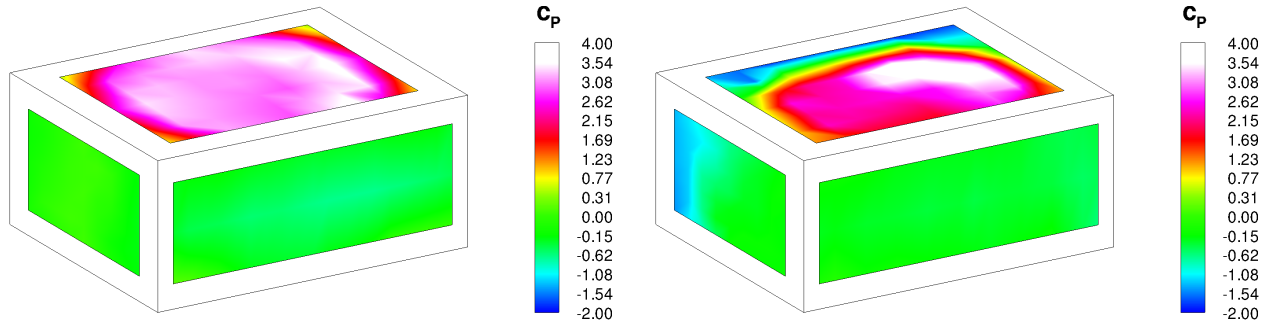

(a) $X/R = -1, Y/R = 0,\ Z/R = 2.\ \mu = 0$

(b) $X/R = -1, Y/R = 0,\ Z/R = 2.\ \mu = 0.05$

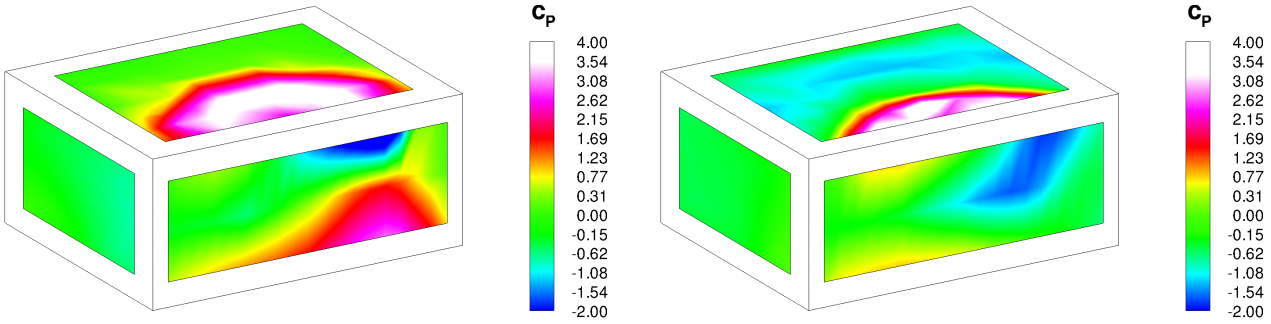

(c) $X/R = 0, Y/R = 0,\ Z/R = 2.\ \mu = 0$

(d) $X/R = 0, Y/R = 0,\ Z/R = 2.\ \mu = 0.05$

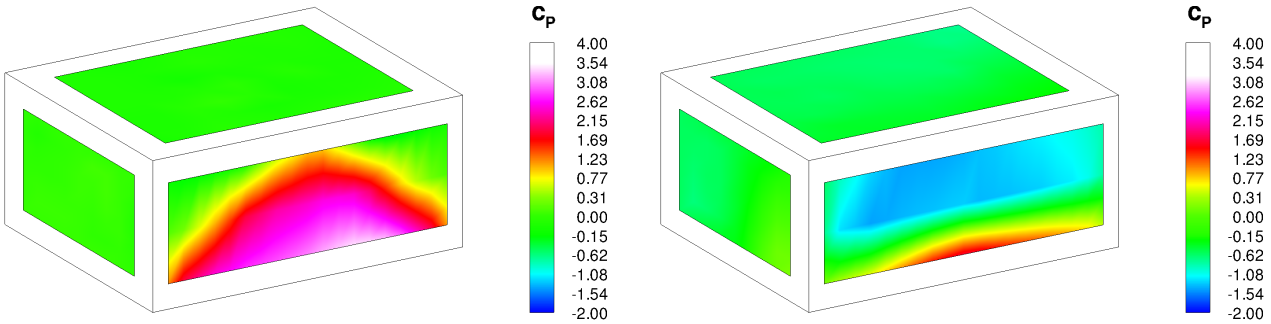

(e) $X/R = 1, Y/R = 0,\ Z/R = 2.\ \mu = 0$

(f) $X/R = 1, Y/R = 0,\ Z/R = 2.\ \mu = 0.05$

Figure 6: Test T2 - Pressure coefficient contours for different helicopter longitudinal positions. Comparison between wind-off ($\mu = 0$, left) and wind-on ($\mu = 0.05$, right) tests.

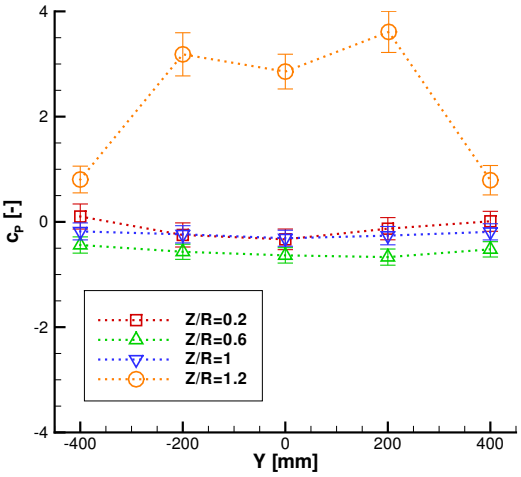

(a) Rotor at $X/R = -1, Y/R = 0$, $Z/R = 2$. $\mu = 0$

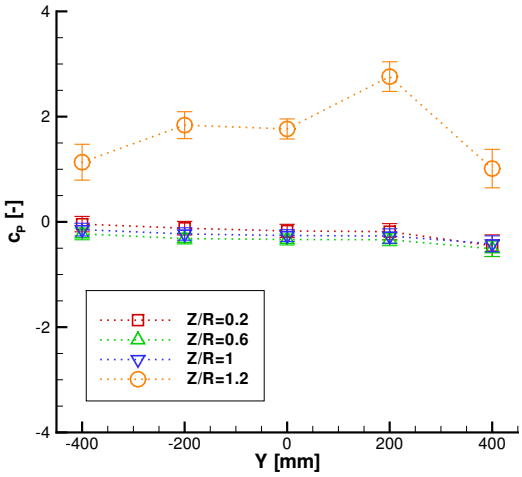

(b) Rotor at $X/R = -1, Y/R = 0$, $Z/R = 2$. $\mu = 0.05$

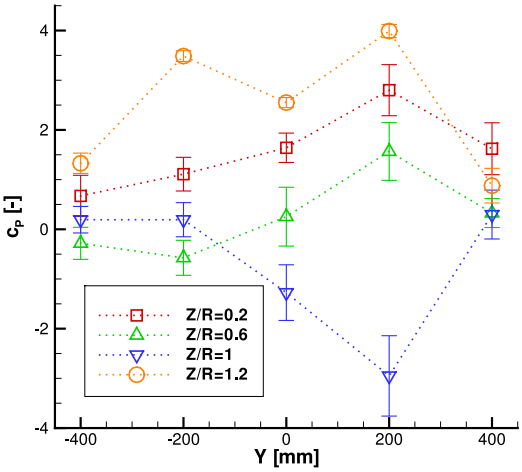

(c) Rotor at $X/R = 0, Y/R = 0$, $Z/R = 2$. $\mu = 0$

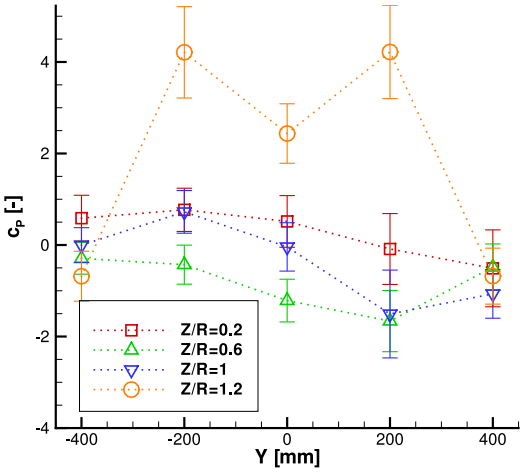

(d) Rotor at $X/R = 0, Y/R = 0$, $Z/R = 2$. $\mu = 0.05$

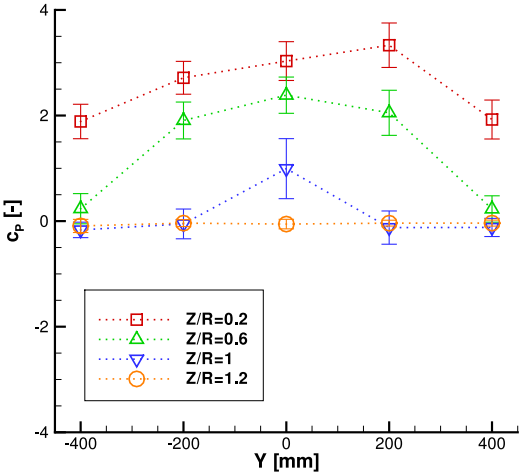

(e) Rotor at $X/R = 1, Y/R = 0$, $Z/R = 2$. $\mu = 0$

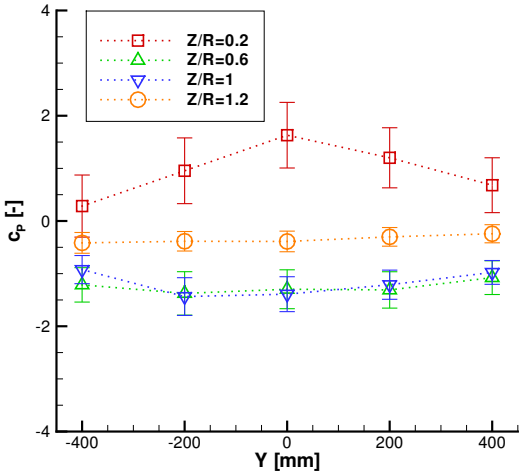

(f) Rotor at Rotor at $X/R = 1, Y/R = 0$, $Z/R = 2$. $\mu = 0.05$

Figure 7: Test T2 - Averaged pressure coefficient and standard deviation of the pressure coefficient (represented as error bar) measured by the Kulite transducers for various rotor positions. Comparison between wind-off ($\mu = 0$, left) and wind-on ($\mu = 0.05$, right) tests.

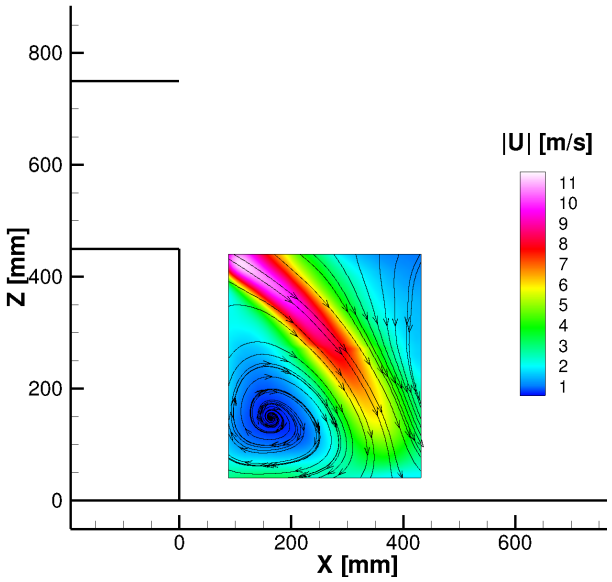

(a) $X/R = -1, Y/R = 0,\ Z/R = 2.\ \mu = 0$

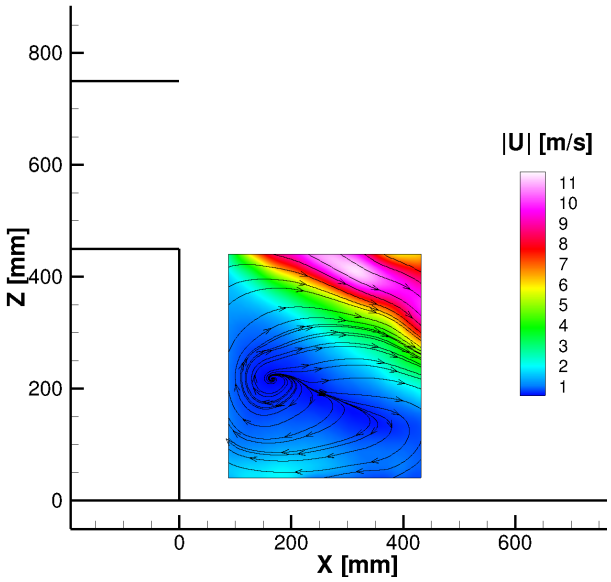

(b) $X/R = -1, Y/R = 0,\ Z/R = 2.\ \mu = 0.05$

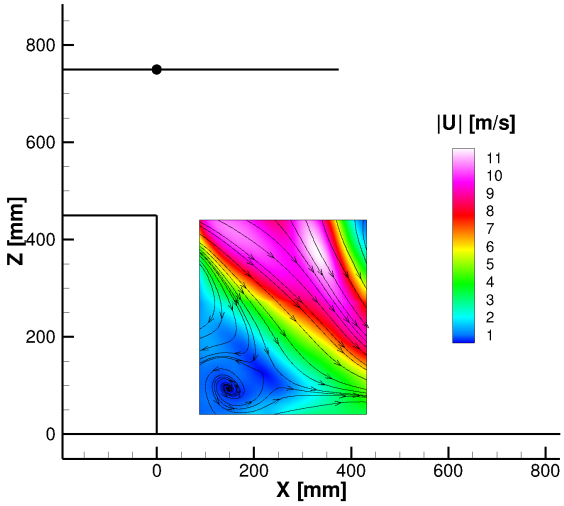

(c) $X/R = 0, Y/R = 0,\ Z/R = 2.\ \mu = 0$

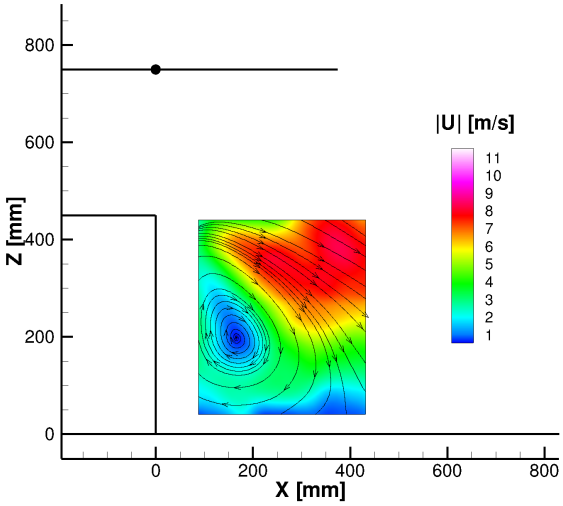

(d) $X/R = 0, Y/R = 0,\ Z/R = 2.\ \mu = 0.05$

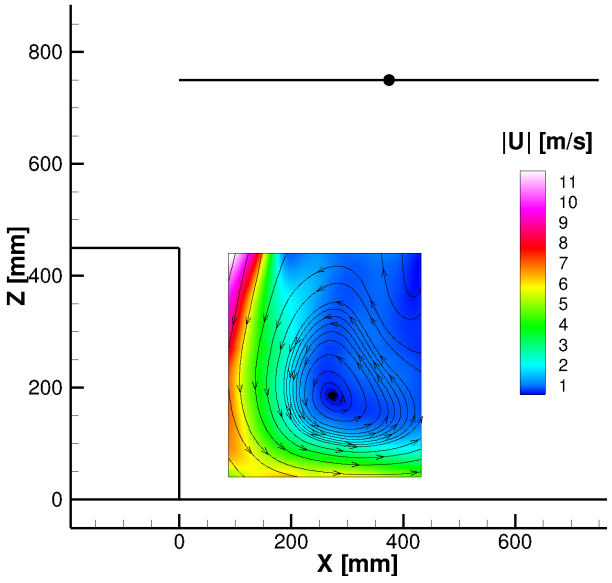

(e) $X/R = 1, Y/R = 0,\ Z/R = 2.\ \mu = 0$

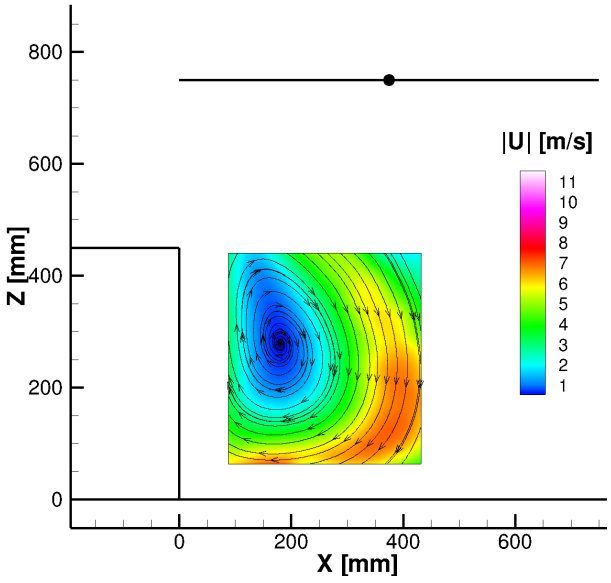

(f) $X/R = 1, Y/R = 0,\ Z/R = 2.\ \mu = 0.05$

Figure 8: PIV results for test T2: In-plane velocity magnitude contours and streamlines. Comparison between wind-off ($\mu = 0$, left) and wind-on ($\mu = 0.05$, right) tests.